

PACS numbers: 42.65.Ky; 42.65.Re; 52.38.Ph
DOI: 10.1070/QE2015v045n05ABEH015789

Control of the photoelectron dynamics for the effective conversion of short-pulse, frequency-modulated optical radiation into X-ray radiation

A.A. Silaev, O.V. Meshkov, M.Yu. Emelin, N.V. Vvedenskii, M.Yu. Ryabikin

Abstract. **We report a theoretical investigation of high-order harmonic generation (HHG) in the ionisation of atoms by nonlinear frequency-modulated laser pulses of short duration. It is shown that the reduction in the instantaneous value of the laser pulse frequency can lead to a significant increase in the width of the plateau in the HHG spectrum. We have found optimal parameters of frequency modulation at which photons with energies of 1 keV are efficiently generated at a relatively low laser-pulse intensity. High HHG efficiency at optimal parameters is explained by the peculiarities of atomic ionisation dynamics and acceleration of photoelectrons by a frequency-modulated laser field.**

Keywords: *frequency-modulated radiation, femtosecond pulses, atoms, ionisation, high harmonic generation, X-rays, attosecond pulses, numerical simulation.*

1. Introduction

One of important directions of research in femtosecond optics is the synthesis of ultrashort optical waveforms for generation of pulses with an arbitrary time dependence of the electric field [1, 2]. In particular, a significant progress has been made in the generation of pulses with a predetermined envelope shape and in the control of changes in the instantaneous value of the electric field at a scale smaller than one period of its oscillation (see, for example, [3] and references therein). Progress in this field is associated with the development of technology of generation of broadband pulses [4], the manipulation of relative phases and amplitudes of the different spectral components of laser radiation and their coherent summation. For example, the authors of [2, 5, 6] have demonstrated the generation and measurement of pulses with controlled subfemtosecond changes in the electric field, based on the synthesis of the waveforms from a spectral continuum or a quasi-continuum extending to 1.5–2 octaves.

Optical waveform shaping allows the complete steering of the microscopic dynamics of electrons and other charged particles in the ionisation of atoms and molecules by laser pulses. In particular, first experiments have been successfully performed to demonstrate the use of these pulses to control the process of ionisation of atoms with subfemtosecond accuracy [6]. This allows one to effectively excite emitting electron currents generated in the produced plasma at different frequencies, which can range from the terahertz [7–9] to vacuum ultraviolet (VUV) and X-ray bands [10–14]. Research in this direction attracts attention due to the possibility of controlling the generation of attosecond pulses, which have broad prospects for the use in various applications, including ultrahigh-time-resolution spectroscopy [11–13].

Emitting high-frequency currents, responsible for the generation of VUV and X-ray radiation in gases, are excited due to ultrafast detachment of electrons from atoms, acceleration of electrons and their recollisions with parent ions [14]. The spectrum of dipole acceleration (proportional to the derivative of the electron current density) contains a high-frequency plateau with a sharp cutoff near a certain frequency ω_c. In the case of a monochromatic laser field [15]

$$\omega_c \approx (I_p + 3.17U_p)/\hbar, \tag{1}$$

where I_p is the ionisation potential of the atom; U_p is the ponderomotive energy of the electron; $\hbar$ is Planck's constant; and the spectrum of dipole acceleration consists of odd harmonics of the pump frequency. Thus, the width of the plateau in the spectrum of high harmonic generation (HHG) is determined by the ponderomotive energy of the electron in the laser field, which is proportional to the product of laser intensity I to the square of its wavelength λ:

$$U_p = e^2E_0^2/(4m\omega_{las}^2) \sim I\lambda^2, \tag{2}$$

where e and m are the charge and mass of the electron; and E_0 and ω_{las} are the amplitude and frequency of laser radiation. It is evident that for the plateau to be extended, one can increase the wavelength of the laser pulse and its intensity. However, generation of intense high-energy harmonics by long-wavelength laser sources is seriously hampered by a rapid decrease in the high-frequency atomic response with increasing laser wavelength [16–18]. This largely stems from the fact that the electron wave packet spreads at the stage of free motion and also that with increasing wavelength atomic levels are strongly depopulated during the laser field period. Increasing the plateau width by increasing the laser pump intensity also has restrictions related to the rapid growth of the rate of tunnelling ionisation of atoms with an increase in the electric field of the laser pulse, resulting in a sharp reduction in the number of atoms involved in the process of harmonic generation [19, 20].

A.A. Silaev, M.Yu. Emelin, N.V. Vvedenskii, M.Yu.Ryabikin Institute of Applied Physics, Russian Academy of Sciences, ul. Ul'yanova 46, 603950 Nizhnii Novgorod, Russia; Lobachevsky State University of Nizhnii Novgorod, prosp. Gagarina 23, 603950 Nizhnii Novgorod, Russia; e-mail: emelin@ufp.appl.sci-nnov.ru, vved@appl.sci-nnov.ru, mike@ufp.appl.sci-nnov.ru;
O.V. Meshkov Lobachevsky State University of Nizhnii Novgorod, prosp. Gagarina 23, 603950 Nizhnii Novgorod, Russia

Received 22 February 2015
Kvantovaya Elektronika **45** (5) 393–400 (2015)
Translated by I.A. Ulitkin

According to the three-stage model of high harmonic generation [14, 21], in the regime of tunnelling ionisation the main role in this process is played by free-bound transitions. Therefore, the effective HHG requires a high enough population of both bound and free states. In the limiting case corresponding to a very small population of the bound states, effective HHG does not occur.

When using pulses with a specially chosen waveform, one can overcome these difficulties and significantly expand the plateau in the spectrum of the electron current, as well as increase the spectral intensity of higher harmonics. In particular, some authors (see, for example, [22, 23]) discuss the use of pulses with nonlinear frequency modulation, which corresponds to a decrease in the instantaneous value of the frequency in the maximum of the laser pulse envelope. A local decrease in frequency leads to an increase in the kinetic energy of photoelectrons at the moment when they return to the ion and thus to an increase in the cutoff frequency ω_c. Note that the spectrum of dipole acceleration is continuous, unlike the case of quasi-monochromatic pulses; however, in accordance with the established terminology, the excitation of the high-frequency electron current by chirped laser pulses is also called high harmonic generation.

This paper investigates optimal HHG conditions in the ionisation of a gas by chirped laser pulses. Using the numerical calculations in the framework of a one-dimensional (1D) quantum-mechanical model and the analytical treatment by a modified Lewenstein model, we have found the optimal parameters of laser pulses, corresponding to the maximum HHG efficiency in the high-frequency domain. It is shown that by using chirped laser pulse the conversion efficiency to higher harmonics may be an order of magnitude higher than in the absence of frequency modulation. Considering the population dynamics of the atomic ground state and using the time-frequency analysis of the high-frequency response of the system, we explain the high efficiency of nonlinear frequency conversion in the found optimal HHG regime by the peculiarities of the dynamics of electron photodetachment and acceleration in this regime. We have also estimated the duration of attosecond pulses which can be obtained using laser pulses with a strong nonlinear frequency modulation, and it is shown that this duration can reach ten attoseconds.

2. Statement of the problem

In this paper it is assumed that the electric field of a chirped laser pulse is linearly polarised along the z axis and is parameterised in the same way as in [22–24]

$$E(t) = E_0 \cos(\omega_{las} t + \delta(t) + \varphi) \exp\left(-2 \ln 2 \frac{t^2}{\tau_p^2}\right). \quad (3)$$

Here τ_p is the pulse duration; φ is the carrier-envelope phase; and

$$\delta(t) = -\Delta\omega \tau_{ch} \tanh\left(\frac{t - t_0}{\tau_{ch}}\right) \quad (4)$$

is the time profile of the carrier-envelope phase, which specifies the pulse frequency modulation. The parameters $\Delta\omega$ and τ_{ch} in (4) determine the amplitude and time scale of frequency modulation; t_0 is the instant of time at which the instantaneous frequency, defined as a derivative of the field phase, deviates from the centre frequency by a maximum value of $\Delta\omega$. Note that for a chirped laser the concept of pulse intensity, generally speaking, does not make sense, because the carrier frequency of the pulse is not constant. Nevertheless, we will use below the quantity of peak intensity, which is represented by $I = cE_0^2/(8\pi)$, where c is the speed of light.

The time-dependent and z-axis-directed dipole acceleration $a(t)$, which is acquired by an atomic electron due to its interaction with the electric field, is calculated using the Ehrenfest theorem [25]:

$$a(t) = \frac{e}{m} E(t) - \frac{1}{m} \left\langle \psi \left| \frac{\partial V}{\partial z} \right| \psi \right\rangle, \quad (5)$$

where ψ is the wave function of an atomic electron; $V(\boldsymbol{r})$ is the Coulomb potential created by the parent ion; and $\boldsymbol{r}$ is the radius vector defining the position of the electron relative to the Coulomb centre. The squared modulus of the Fourier expansion coefficient of the dipole acceleration (the HHG spectrum)

$$a_\omega = \int_{-\infty}^{\infty} a(t) \exp(-i\omega t)\, dt \quad (6)$$

determines the spectral intensity of the generated high-frequency radiation. To find the optimal parameters of frequency modulation the so-called HHG power is calculated, equal to the integral of $|a_\omega|^2$ over frequencies in some spectral range:

$$W = \int_{\omega_{min}}^{\omega_{max}} |a_\omega|^2\, d\omega. \quad (7)$$

The positions of the boundaries ω_{min} and ω_{max} of the spectral range in question will be specified in Sections 3 and 4.

3. Numerical calculations

3.1. Methods of calculation

At the first stage of this research, to accelerate calculations when searching for the optimal parameters of chirped laser pulses we used a 1D quantum-mechanical model of the hydrogen atom, proposed in [10]. Using this model involves the solution of a 1D time-dependent Schrödinger equation (TDSE)

$$i\hbar \frac{\partial \psi}{\partial t} = -\frac{\hbar^2}{2m} \frac{\partial^2 \psi}{\partial z^2} + V_{1D}(z)\psi - ezE(t)\psi, \quad (8)$$

where

$$V_{1D}(z) = -\frac{e^2}{(|z|^{1/2} + 0.6 r_B^{1/2})^2} \quad (9)$$

is the model (the so-called supersolid-core) potential; and $r_B = 5.29 \times 10^{-9}$ cm is the Bohr radius. The energy of the ground state in this potential is equal in absolute value to the ionisation potential of the hydrogen atom ($I_p = 13.6$ eV), and the potential itself is asymptotically close to the Coulomb potential away from the ion. The use of this potential provides high accuracy in describing the stage of ionisation of an atom, which is essential for the research conducted in this paper.

In some cases, the results obtained in 1D model calculations as well as in the analytical consideration (Section 4) were compared with the results of three-dimensional (3D) numerical calculations. Taking into account the axial symmetry of the problem, the 3D TDSE was numerically integrated in the cylindrical coordinate system (ρ,θ,z), in which it is written as

$$i\hbar\frac{\partial\psi}{\partial t} = -\frac{\hbar^2}{2m}\left[\frac{\partial^2\psi}{\partial\rho^2} + \frac{1}{\rho}\frac{\partial}{\partial\rho} + \frac{\partial^2}{\partial z^2}\right]\psi + [V(\rho,z) - ezE(t)]\psi, \quad (10)$$

where $V(\rho,z)$ is the Coulomb potential of the ion.

The numerical integration of the TDSE in the 1D and 3D cases was performed by using the pseudospectral method [26]. To transform the wave function from the coordinate representation to the momentum representation and back, we use a fast Fourier transform in the 1D problem and a fast Fourier transform along the z axis and a discrete Fourier–Bessel transform along ρ in the 3D problem. The calculations were performed in the domains $z_{min} \leqslant z \leqslant z_{max}$ (1D problem) and $z_{min} \leqslant z \leqslant z_{max}$, $0 \leqslant \rho \leqslant 64r_B$ (3D problem). To suppress the reflection of the wave function from the boundaries of the computational domain and emerging wave packets on the opposite edge of the grid, use is made of the absorption of the wave function on the periphery of the computational domain. The values of z_{min} and z_{max} were determined based on the solutions of the classical equations of motion of the electron so that the electrons born at arbitrary time instants and returning to the ion do not fall into the absorbing layer during the motion. In solving the 1D TDSE, a step Δz along the coordinate was chosen equal to $0.15r_B$. In solving the 3D TDSE, we used an equidistant grid along z with a step $\Delta z = 0.23r_B$, while the nodes of the grid along ρ were located nonequidistantly: they become condensed with approaching $\rho = 0$, and their total number N_ρ is equal to 420. The integration over time is performed in the domain $-t_{max} \leqslant t \leqslant t_{max}$, where $t_{max} = 3.5\tau_p$ with a step $\Delta t = 0.015t_a$, where $t_a = 2.42 \times 10^{-17}$ s is the atomic unit of time.

3.2. Calculation results

Here we consider the problem of finding the parameters of a chirped laser pulse, at which the HHG power W is maximal in a semi-infinite spectral range $\omega > \omega_{min}$, where $\hbar\omega_{min} = 800$ eV. It is assumed that the amplitude of the frequency modulation of the laser pulse can take values in a wide range $0 \leqslant \Delta\omega \leqslant \omega_{las}$. The peak intensity I of the pulse is set equal to 6×10^{14} W cm^{-2}, the duration $\tau_p = 5.89$ fs, the unshifted centre wavelength $\lambda = 2\pi c/\omega_{las} = 0.8$ μm, the carrier-envelope phase $\varphi = 0$, and the time scale of the frequency modulation $\tau_{ch} = 4.84$ fs.

To find the optimal values of t_0 and $\Delta\omega$ we used the 1D model described in Section 3.1. Using this model we calculated the values of W in the range $0 \leqslant \Delta\omega \leqslant \omega_{las}$ and a wide range of t_0. The results obtained show that the local maxima W are achieved near the maximum value of the modulation-frequency amplitude $\Delta\omega = \omega_{las}$. The global maximum is reached near $t_0 = 0.82$ fs and $\Delta\omega/\omega_{las} = 0.988$. Figure 1 shows the dependence of W on t_0 at $\Delta\omega/\omega_{las} = 0.988$. One can see that the curve $W(t_0)$ has several sharp peaks alternating with a period 1.4 fs, which approximately corresponds to half the field period at a wavelength of 0.8 μm. In the two peaks located near $t_0 = 0.82$ and 2.3 fs, the value of W takes similar values that significantly exceed the corresponding values in other peaks of the function $W(t_0)$. Also, an interesting feature in the dependence of W on t_0 is a very sharp (many orders of magnitude) drop of $W(t_0)$ at a small (hundredths of a femtosecond) change in t_0. A sudden drop in $W(t_0)$ means that the edge of the plateau crosses the lower boundary ω_{min} of the spectral interval in integral (7). This indicates that the position of the plateau edge in the HHG spectrum varies greatly with a small change in t_0.

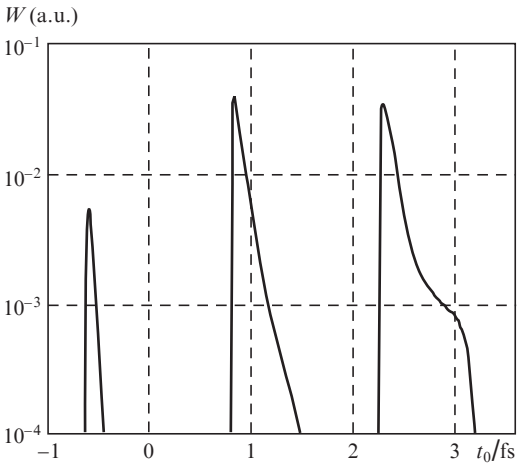

Figure 1. Dependence of the HHG power W in a semi-infinite spectral range $\omega > \omega_{min}$ ($\hbar\omega_{min} = 0.8$ keV) on time t_0, corresponding to the highest modulation frequency, at $I = 6 \times 10^{14}$ W cm^{-2}, $\tau_p = 5.89$ fs, $\lambda = 0.8$ μm, $\varphi = 0$, $\tau_{ch} = 4.84$ fs and $\Delta\omega/\omega_{las} = 0.988$.

Next, we performed a 3D numerical integration of the TDSE for the chirped pulse parameters, which correspond, according to the 1D calculation in Fig. 1, to one of the most intense peaks (at $\Delta\omega/\omega_{las} = 0.988$, $t_0 = 0.82$ fs). One can see from Fig. 2, where the black line shows the HHG spectrum for this case, that the photon energy corresponding to the plateau edge is $\hbar\omega_c \approx 890$ eV (far exceeding the value of the cutoff energy, obtained in [22]). Thus, short chirped laser pulses with a relatively low intensity can be used to generate radiation with photon energies on the order of 1 keV.

Let us now consider how the spectral densities of the dipole acceleration in the region of the plateau edge correlate in the case of a chirped pulse and a pulse without frequency modulation. The gray line in Fig. 2 shows the HHG spectrum calculated for a pulse with $\delta = 0$ when the values of I, τ_p and φ are the same as those for a chirped pulse, but at a longer centre wavelength ($\lambda = 2.234$ μm). One can see from Fig. 2 that in both cases the HHG spectrum extends almost to 0.9 keV, but in the case of a frequency-modulated pulse the conversion efficiency to higher harmonics is almost an order of magnitude higher than in the absence of frequency modulation.

This significant difference in the output of harmonics is explained by significant differences in temporal changes in the electric field inside the specified envelope for the two pulses in question (Fig. 3). Because of the strong dependence of the ionisation rate of the electric field [27], these differences lead to a significant difference in the ionisation dynamics and, as a result, in a time-frequency evolution of the HHG process.

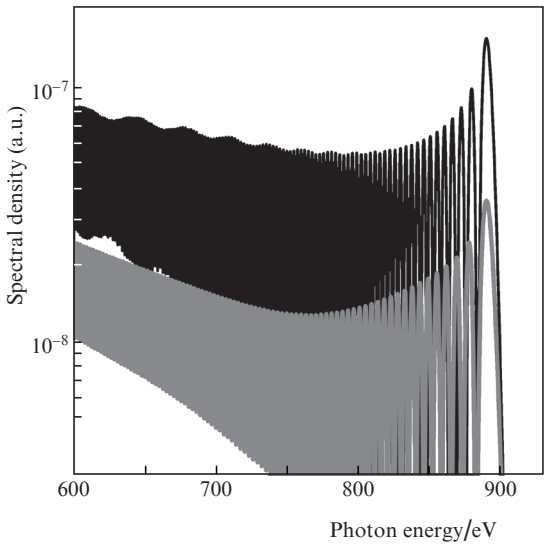

Figure 2. HHG spectra in the high-frequency region for a chirped laser pulse (black curve) and a pulse without frequency modulation (gray curve) at $I = 6 \times 10^{14}$ W cm^{-2}, $\tau_p = 5.89$ fs, $\varphi = 0$ and $\lambda = 0.8$ μm (with frequency modulation) and 2.234 μm (without it); the parameters of the chirped pulse frequency modulation are: $\tau_{ch} = 4.84$ fs, $\Delta\omega/\omega_{las} = 0.988$ and $t_0 = 0.82$ fs.

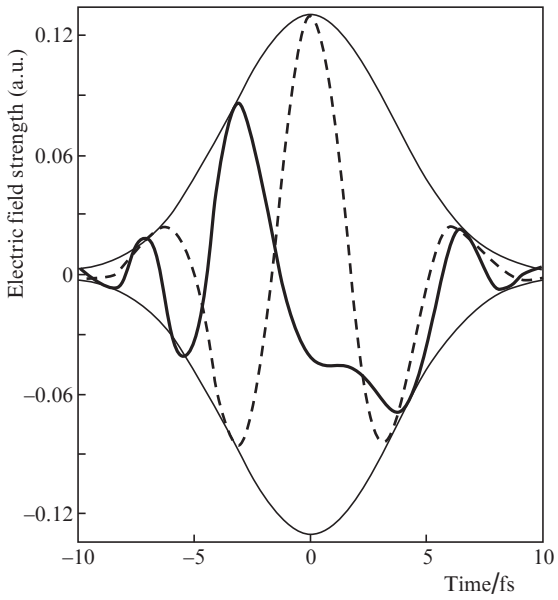

Figure 3. Time profiles of the electric field of pulses with frequency modulation (solid curve) and without it (dashed curve), which correspond to HHG spectra plotted in Fig. 2.

To show this, let us consider the results of the calculations shown in Fig. 4. Figure 4a shows the time dependence of the ground state population of the atoms:

$$P_0(t) = |\langle\psi|\psi_0\rangle|^2, \qquad (11)$$

where $\psi_0(\boldsymbol{r})$ is the wave function of the ground state. Figures 4b and 4c show wavelet spectrograms of the dipole acceleration, which provide a time-frequency analysis of the high-frequency response of the system. To calculate the spectrogram we used the formula

$$S(t,\Omega) = \sqrt{\frac{\Omega}{\tau_0}}\int_{-\infty}^{\infty} a(t-t')\exp\left(-i\Omega t' - \frac{\Omega^2 t'^2}{2\tau_0^2}\right)dt', \qquad (12)$$

where $\tau_0 = 5\pi/\sqrt{\ln 4} \approx 13.34$ (see, for example, [28, 29]). As follows from Fig. 4a, both pulses, depicted in Fig. 3, quite strongly ionise the gas near the time instant $t \approx -3$ fs, corresponding to the local maxima of the electric field modulus. Further dynamics of the electrons for these two pulses markedly varies.

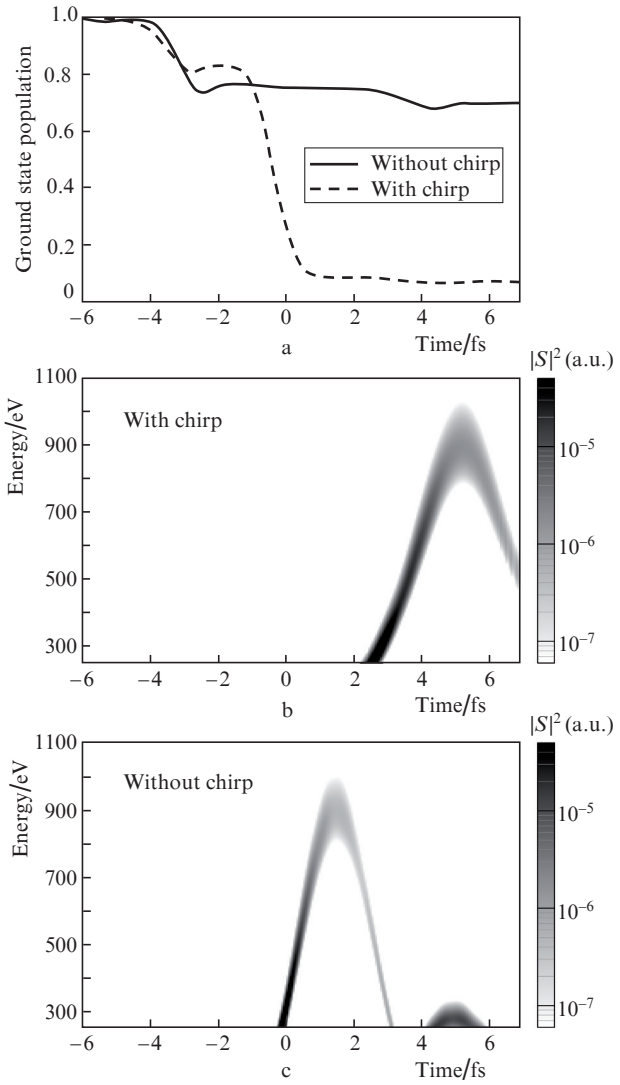

Figure 4. (a) Time dependences of the ground state population P_0 of the atom and wavelet spectrograms $S(\Omega, t)$ of the dipole acceleration for pulses (b) with frequency modulation and (c) without it, as shown in Fig. 3.

In the case of a pulse without frequency modulation, the electric field strength amplitude in the next half-cycle after the electron detachment increases. By the time $t \approx 1.5$ fs, when part of the wave packet corresponding to the most high-energy free electrons returns to the parent ion, the ground state under the influence of this field is almost completely depleted (see Fig. 4a, dashed curve), which leads to the fact that the excited high-frequency electron current is weak.

In using a chirped pulse, the population P_0 of the ground state remains almost unchanged in the time interval between

detachment and return of the high-energy electron (Fig. 4a, solid curve) and corresponds to approximately 70% of the total number of electrons. Because the field near the envelope maximum changes slower than at the leading edge (Figure 3, solid curve), the photoelectrons by the time of their return acquire a large enough energy. Since the population of both free and bound states in this case is sufficiently high, the high-frequency polarisation is excited efficiently and the spectral HHG density is much higher than in the case of a pulse without frequency modulation.

The use of short pulses with a nonlinear frequency modulation allows one to efficiently generate isolated attosecond pulses [22, 23]. To show this, let us consider again the wavelet spectrogram of dipole acceleration for a chirped pulse (Fig. 4b). As can be seen from the figure, high frequencies in dipole acceleration are excited on a separate time interval with a duration determined by the time of return of electrons produced on the same crest of the electric field at $t \approx -3$ fs. This duration in the case under study is a few femtoseconds, which is related to the fact that the phases of different spectral components of dipole acceleration greatly differ from each other.

The duration of the generated high-frequency pulse can be reduced using a selection of 'short' trajectories of electrons and chirp compensation of the generated radiation [30]. 'Short' and 'long' trajectories of electrons (called so in accordance with the time of motion of electrons in the continuum) correspond to different parts (positive and negative frequency chirps) of the spectrogram. In selecting only short trajectories, the frequency chirp of dipole acceleration is positive and close to linear, i.e., $\omega(t) \approx \alpha t + \beta$, where $\alpha > 0$ and β are some coefficients. Because the phase of the spectral components of dipole acceleration is determined by the integral of the frequency over time, it has a term $\Delta\phi$, quadratic in frequency $\omega(t)$: $\Delta\phi = \omega^2/2\alpha$. The corresponding frequency quadratic phase portion of the generated radiation can be compensated for by transmitting radiation through a thin plate (or a set of plates) made of a metal having anomalous dispersion in the passband [30–32].

Let us estimate what duration of the attosecond pulse we can thus obtain in the case of a chirped laser pulse (with the parameters specified in the caption to Fig. 2). To do this, we conduct the following transformation of dipole acceleration $a(t)$. For the 'short' trajectories to be selected, the function $a(t)$ is multiplied by the mask function equal to zero in the time interval, corresponding to 'long' trajectories, and to unity in the time interval, corresponding to 'short' trajectories. From the Fourier spectrum of the resulting function we subtract the phase $\Delta\phi = \omega^2/2\alpha$, where $\alpha = 0.28t_a^{-2}$ (the value of this coefficient was found from the wavelet spectrogram), and filter out the low-frequency portion of the photons with energies below 420 eV. The square of the modulus of the inverse Fourier transform coefficients of the resulting signal corresponds to the square $E_{ap}^2(t)$ of the electric field generated as an attosecond pulse. Figure 5 shows the time dependence of E_{ap}^2, shifted to zero along the t axis. It can be seen that the characteristic duration of the generated attosecond pulse is ~13 as. This result demonstrates that using frequency-modulated laser pulses one can achieve a significant decrease in the attosecond pulse duration.

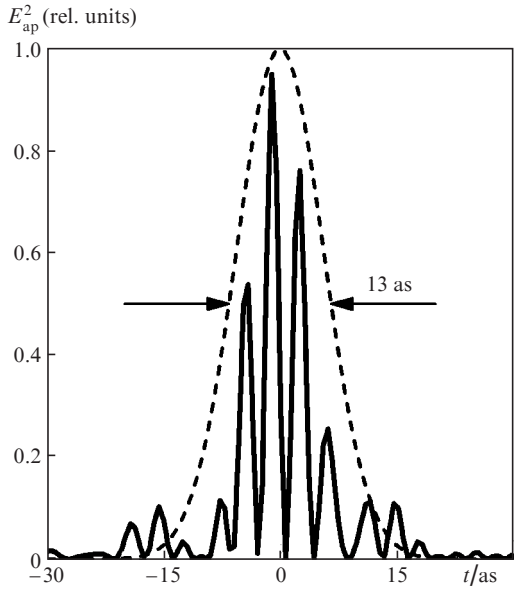

Figure 5. Time profile of the square of the electric field of an attosecond pulse produced by HHG using frequency-modulated radiation with the parameters specified in the caption to Fig. 2. The attosecond pulse is produced using the selection of 'short' trajectories of electrons involved in the HHG and compensation of the positive chirp of the frequency of the generated radiation.

4. Analytical description

The solution to the problem of finding the parameters of a frequency-modulated laser pulse presented in Section 3 to implement the optimal HHG regime was based on the use of numerical calculations in the framework of the quantum-mechanical model, i.e., on the numerical solution of the 1D TDSE. However, if there are more than two variable laser pulse parameters, the use of this approach to solve the optimisation problem requires much time and significant computing resources. This makes it necessary to use alternative (usually approximate) approaches in such problems. One of these approaches is any of semi-analytic quantum-mechanical theories [21, 33, 34], allowing one, in the framework of certain approximations, to represent the sought-for high-frequency polarisation response of the system under study in an integrated form. Below we use Lewenstein's theory [21], modified so as to take into account the important effect of the depletion of atomic levels by an intense laser field.

4.1. Modified strong-field approximation

Lewenstein's theory [21] provides a quantum-mechanical description of a three-step HHG process [14] in the strong-field approximation. In this theory, the wave function of an electron interacting with an intense electromagnetic field has the form of a superposition of the unperturbed eigenfunction of the ground bound state in the atom and set of continuous spectrum functions given, in accordance with the strong-field approximation, in the form of plane waves without taking into account the influence of the Coulomb potential. The time-dependent mean dipole moment of the system is expressed in this case as an integral in time and components of a canonical momentum of the electron, containing a rapidly oscillating integrand factor in the form of an exponential, whose exponent is given by the electron's quasi-classical action $S(\boldsymbol{p}, t, t')$ ($\boldsymbol{p}$ is the canonical momentum of the electron, t is the current time and t' is a temporary variable of integration). The main contribution to the momentum inte-

grals are given by stationary points of action: $\nabla_{\boldsymbol{p}} S(\boldsymbol{p}, t, t') = 0$. These stationary points have a clear physical meaning: their contribution to the high-frequency nonlinear response of the system corresponds to free-electron trajectories, beginning at the nucleus and ending at the same nucleus later; this picture is consistent with the assumptions of the semiclassical model [14]. The theory [21] provides not only qualitative but also quantitative confirmation of the main conclusions of the semiclassical model, showing, in particular, good agreement with it, regarding the position of cutoff energy (1) in the HHG spectrum.

The original version of Lewenstein's theory was constructed on the assumption of weak ionisation, i.e., the population of the ground state was considered unchanged. Further development of the HHG theory showed that accounting for the depopulation of the bound state can be reduced to the multiplication of the probability amplitudes of the electron transitions from the ground state to the continuum at time $t-\tau$ and from the continuum to the ground state at time t by the amplitude of the ground state at time moments $t-\tau$ and t, respectively, where τ is the time of the electron motion in free space. This changing amplitude of the ground state can be approximately calculated as

$$a(t) = \exp\left[-\int_{-\infty}^{t} \frac{w(t')}{2} \mathrm{d}t'\right],$$

where $w(t')$ is the time-dependent ionisation rate. As a result, the expression for the variable dipole moment of the atom in an external linearly polarised electromagnetic field has the form (hereinafter atomic units are used):

$$z(t) = \mathrm{i}\int_0^t \mathrm{d}\tau \left(\frac{\pi}{\varepsilon + \mathrm{i}\tau/2}\right)^{3/2} d_z^*[p_{\mathrm{st}}(t,\tau) - A_z(t)]$$

$$\times d_z[p_{\mathrm{st}}(t,\tau) - A_z(t-\tau)] E(t-\tau)$$

$$\times \exp\left[-\mathrm{i}S_{\mathrm{st}}(t,\tau) - \int_0^t \frac{w(t')}{2}\mathrm{d}t' - \int_0^{t-\tau} \frac{w(t')}{2}\mathrm{d}t'\right] + \text{c.c.} \quad (13)$$

Here, $\boldsymbol{A}(t) = \boldsymbol{e}_z A_z(t)$ is the vector potential of the electromagnetic field of the laser pulse; $\boldsymbol{e}_z$ is the unit vector along the z axis; ε is the regularisation parameter, which may be selected small;

$$p_{\mathrm{st}}(t,\tau) = \frac{1}{\tau}\int_{t-\tau}^{t} \frac{A_z(t')}{c}\mathrm{d}t' \quad (14)$$

is the z coordinate of a stationary point [$\nabla_{\boldsymbol{p}} S_{\mathrm{st}}(\boldsymbol{p}, t, \tau) = 0$] of the quasi-classical action, describing the free motion of an electron in the field of the laser pulse:

$$S(\boldsymbol{p}, t, \tau) = \int_{t-\tau}^{t} \left[\frac{1}{2}\left(\boldsymbol{p} - \frac{\boldsymbol{A}(t')}{c}\right)^2 + I_{\mathrm{p}}\right]\mathrm{d}t'; \quad (15)$$

the stationary value of the z-component of the canonical momentum of the electron, $\boldsymbol{p}$, corresponds to the classical trajectory starting at the nucleus at time $t-\tau$ and ending on it at time t; $S_{\mathrm{st}}(t,\tau)$ is the quasi-classical action corresponding to $p_{\mathrm{st}}(t,\tau)$; and $d_z(\boldsymbol{p})$ is the component of the dipole matrix element corresponding to the transition from the ground bound state into the continuous spectrum. For hydrogen-like systems in which highly excited states in the continuum can be approximately regarded as plane waves, the matrix element has the form

$$d_z(\boldsymbol{p}) = \mathrm{i}\frac{2^{7/2}(2I_{\mathrm{p}})^{5/4}}{\pi}\frac{p_z}{(\boldsymbol{p}^2 + 2I_{\mathrm{p}})^3}. \quad (16)$$

To calculate the value of $w(t)$, which is responsible for the depletion of the nonlinear medium, various approaches [21, 35–37] were proposed. It is known from the literature [38, 39] that the widely used formula for the tunnelling ionisation rate [40], at large values of $|E|$ (of interest to us in this problem), greatly overestimates its value. Therefore, following [37], in the present study we calculate $w(t)$ by using an analytical formula for the tunnelling ionisation rate of an atom in a static field, corrected for above-barrier regime proposed in [39]:

$$w(t) = C_l^2 \left(\frac{4I_{\mathrm{p}}}{|E(t)|}\right)^{2Z/\sqrt{2I_{\mathrm{p}}}-1} \exp\left[-\frac{2(2I_{\mathrm{p}})^{3/2}}{3|E(t)|}\right]$$

$$\times \exp\left[-\frac{6Z^2|E(t)|}{I_{\mathrm{p}}(2I_{\mathrm{p}})^{3/2}}\right]. \quad (17)$$

Here, C_l is the numerical coefficient, which is determined from the condition of the wave function normalisation; and Z is the effective nuclear charge. The last exponential factor in (17) is the aforementioned correction factor that allows one, as shown in [39], to calculate with high accuracy the ionisation rate of atoms in a wide range of electric-field strengths E.

4.2. Calculation results

The results presented below were obtained within the framework of the modified strong-field approximation described in Section 4.1. Here we consider the problem of maximising the efficiency of conversion of optical radiation into the 'water window', i.e., the wavelength region between 2.3 and 4.4 nm, which is important for biochemical studies, where carbon-containing biological objects effectively absorb radiation, while water is relatively transparent. Accordingly, in order to find the optimal parameters of the considered laser pulses we calculated the HHG power in the photon energy range from $\hbar\omega_{\min} = 284$ eV to $\hbar\omega_{\max} = 543$ eV. Using the analytic theory instead of direct numerical integration of the TDSE allowed us to investigate the HHG efficiency in a wide range of variable parameters E_0, $\Delta\omega$, t_0, τ_{ch} and φ of a frequency modulated pulse, given by formulas (3) and (4). The unshifted centre wavelength and pulse duration were assumed equal to 0.8 μm and 5 fs. The high-frequency part of the HHG spectrum corresponding to the found optimum set of the parameters is shown in Fig. 6a (black curve). The cutoff energy in this case is about 375 eV.

As in Section 3.2, we compared the efficiency of conversion of optical radiation into the high frequency radiation for cases of a chirped pulse and a pulse without frequency modulation; in the second case, we set the pulse parameters which provide the same position of the plateau edge, as in the case of a chirped pulse. The comparison was carried out for a wide range of unchirped pulse intensities; moreover, since, according to (1) and (2), the position of the plateau edge in the spectra of high harmonics is determined by the product of the laser intensity by the square of its wavelength, we varied the wavelength λ with intensity I (according to the condition of

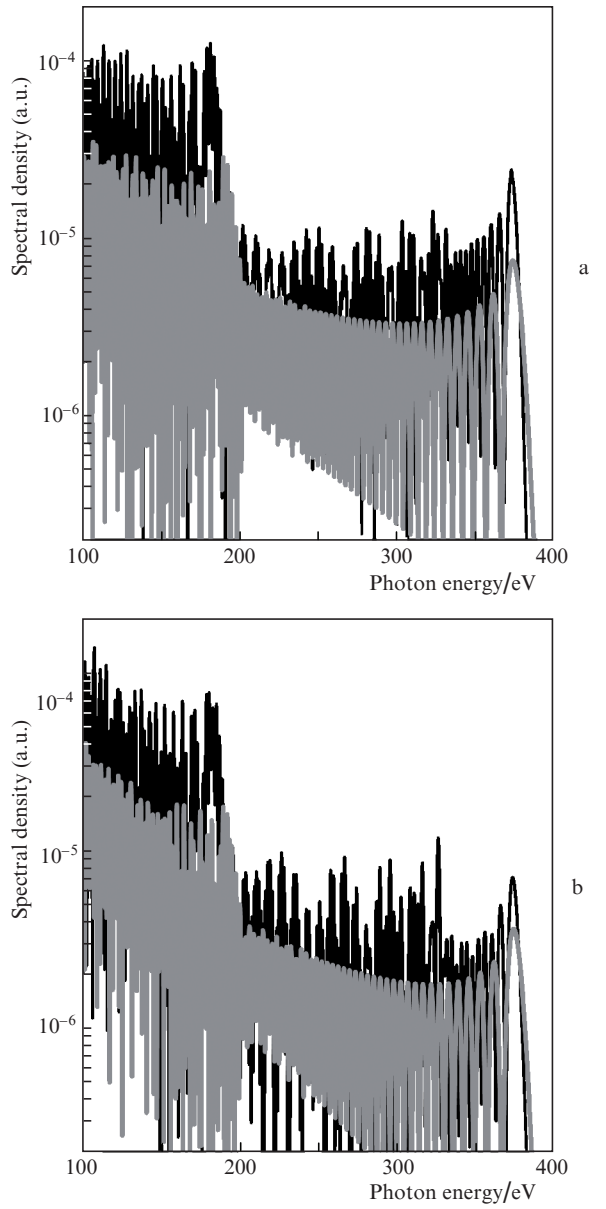

Figure 6. HHG spectra in the high-frequency region for a chirped laser pulse (black curve) at $\tau_p = 5$ fs, $\varphi = 2.9$ rad, $I = 4.5 \times 10^{14}$ W cm^{-2}, $\lambda = 0.8$ μm, $\tau_{ch} = 3.65$ fs, $\Delta\omega/\omega_{las} = 0.75$, $t_0 = 3.06$ fs and a pulse without frequency modulation (gray curve) at $I = 6 \times 10^{14}$ W cm^{-2}, $\lambda = 1.43$ μm. The calculations were performed using (a) the modified strong-field approximation and (b) the solution of the 3D TDSE.

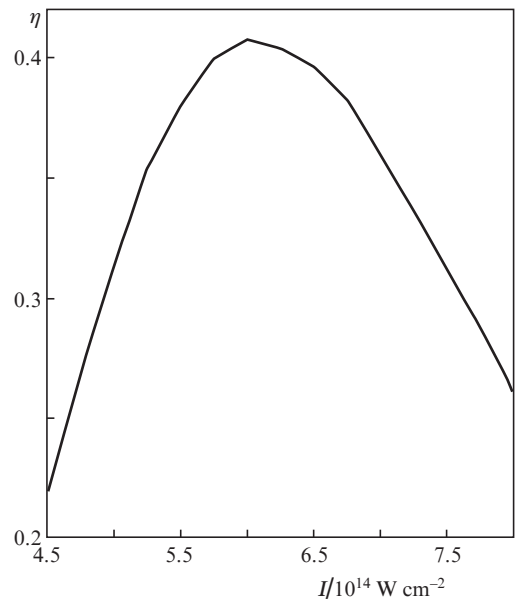

Figure 7. Ratio η of the HHG powers for a laser pulse without frequency modulation and a frequency-modulated pulse as a function of the intensity I of a pulse without frequency modulation with a centre wavelength λ satisfying the condition $I\lambda^2 = \text{const}$. In both cases, the laser pulse duration and cutoff energy in the HHG spectrum are equal to 5 fs and 375 eV.

constant $I\lambda^2$). The results of these calculations are shown in Fig. 7.

Figure 7 shows that in the case of a pulse without frequency modulation the HHG power is 2.4–4.6 times lower than in the case of a chirped pulse. The maximum efficiency of the harmonic generation with the above-mentioned cutoff energy in the case of a pump without frequency modulation is observed at $I \approx 6 \times 10^{14}$ W cm^{-2} and $\lambda \approx 1.43$ μm; the corresponding HHG spectrum is shown in Fig.6a (gray curve). Note that the mentioned optimum pulse intensity without frequency modulation, required for obtaining the energy cutoff of 375 eV, is approximately 1.33 times higher than in the case of a chirped pulse. At lower intensities, the generation of photons with such energies requires longer-wavelength pumping, which, as noted in the Introduction, leads to a decrease in the yield of harmonics, while at higher intensities HHG is suppressed due to the depletion of the nonlinear medium. The HHG spectra given in Fig. 6b, obtained by solving the 3D TDSE, are in good agreement with the results of calculations in the framework of the modified strong-field approximation (Fig. 6a).

An analysis of the dynamics of the ground state population of the atom in the case of pulses with frequency modulation and without it in the considered problem of high harmonic generation in the 'water window' leads to the results similar to those for harmonic generation in the region below 1 keV (Fig. 4a). This indicates a common mechanism, which is responsible for a significant increase in the HHG efficiency in the regimes under study when use is made of laser pulses with strong frequency modulation.

5. Conclusions

We have studied the high-order harmonic generation in the ionisation of the gas by an intense laser pulse with nonlinear frequency modulation. We have found the optimal laser pulse parameters, corresponding to the maximum conversion efficiency of laser radiation into the 'water window' (corresponding to photon energies of 280–540 eV) and into a higher frequency range with photon energies of the order of 1 keV. It is shown that by using a chirped laser pulse the conversion efficiency to higher harmonics may be substantially greater than in the absence of the frequency modulation, and the generated radiation can be converted into isolated ultrashort pulses having a duration of ~ 10 as. The high efficiency of nonlinear frequency conversion in the found optimal HHG regimes is explained by the features of the dynamics of the ionisation process that is characterised in this case by a combination of a high probability of detachment of electrons making the

main contribution to the high-frequency region of the HHG spectrum with a relatively low probability of the depletion of atomic levels in the time interval between the detachment of the electron and its collision with the parent ion.

Acknowledgements. The work was supported by the Presidium of the Russian Academy of Sciences (Extreme Light Fields and Their Applications Programme), Russian Foundation for Basic Research (Grant Nos 14-02-00762 and 14-02-31044), Grant from the Government of the Russian Federation (Agreement No. 14.B25.31.0008) and the RF President's Grants Council (State Support to the Leading Scientific Schools Programme, Grant No. NSh-2001.2014). We are grateful to the Joint Supercomputer Center of the Russian Academy of Sciences and Lobachevsky State University of Nizhni Novgorod for providing computing resources.

References

1. Goulielmakis E., Yakovlev V.S., Cavalieri A.L., Uiberacker M., Pervak V., Apolonski A., Kienberger R., Kleineberg U., Krausz F. *Science*, **317**, 769 (2007).
2. Chan H.-S., Hsieh Z.-M., Liang W.-H., Kung A.H., Lee C.-K., Lai C.-J., Pan R.-P., Peng L.-H. *Science*, **331**, 1165 (2011).
3. Wang X., Jin C., Lin C.D. *Phys. Rev. A*, **90**, 023416 (2014).
4. Goulielmakis E., Schultze M., Hofstetter M., Yakovlev V.S., Gagnon J., Uiberacker M., Aquila A.L., Gullikson E.M., Attwood D.T., Kienberger R., Krausz F., Kleineberg U. *Science*, **320**, 1614 (2008).
5. Huang S.-W., Cirmi G., Moses J., Hong K.-H., Bhardwaj S., Birge J.R., Chen L.-J., Li E., Eggleton B.J., Cerullo G., Kärtner F.X. *Nature Photon.*, **5**, 475 (2011).
6. Wirth A., Hassan M.Th., Grguras I., Gagnon J., Moulet A., Luu T.T., Pabst S., Santra R., Alahmed Z.A., Azzeer A.M., Yakovlev V.S., Pervak V., Krausz F., Goulielmakis E. *Science*, **334**, 195 (2011).
7. Silaev A.A., Vvedenskii N.V. *Phys. Rev. Lett.*, **102**, 115005 (2009).
8. Vvedenskii N.V., Korytin A.I., Kostin V.A., Murzanev A.A., Silaev A.A., Stepanov A.N. *Phys. Rev. Lett.*, **112**, 055004 (2014).
9. Alexandrov L.N., Emelin M.Y., Ryabikin M.Y. *J. Phys. B: At. Mol. Opt. Phys.*, **47**, 204028 (2014).
10. Silaev A.A., Ryabikin M.Y., Vvedenskii N.V. *Phys. Rev. A*, **82**, 033416 (2010).
11. Corkum P.B., Krausz F. *Nature Phys.*, **3**, 381 (2007).
12. Krausz F., Ivanov M. *Rev. Mod. Phys.*, **81**, 163 (2009).
13. Pfeifer T., Abel M.J., Nagel P.M., Jullien A., Loh Z.-H., Bell M.J., Neumark D.M., Leone S.R. *Chem. Phys. Lett.*, **463**, 11 (2008).
14. Corkum P.B. *Phys. Rev. Lett.*, **71**, 1994 (1993).
15. Krause J.L., Schafer K.J., Kulander K.C. *Phys. Rev. Lett.*, **68**, 3535 (1992).
16. Tate J., Auguste T., Muller H.G., Salières P., Agostini P., DiMauro L.F. *Phys. Rev. Lett.*, **98**, 013901 (2007).
17. Colosimo P., Doumy G., Blaga C.I., Wheeler J., Hauri C., Catoire F., Tate J., Chirla R., March A.M., Paulus G.G., Muller H.G., Agostini P., DiMauro L.F. *Nature Phys.*, **4**, 386 (2008).
18. Shiner A.D., Trallero-Herrero C., Kajumba N., Bandulet H.-C., Comtois D., Lègarè F., Giguère M., Kieffer J.-C., Corkum P.B., Villeneuve D.M. *Phys. Rev. Lett.*, **103**, 073902 (2009).
19. Moreno P., Plaja L., Malyshev V., Roso L. *Phys. Rev. A*, **51**, 4746 (1995).
20. Strelkov V.V., Sterjantov A.F., Shubin N.Yu., Platonenko V.T. *J. Phys. B: At. Mol. Opt. Phys.*, **39**, 577 (2006).
21. Lewenstein M., Balcou Ph., Ivanov M.Yu., L'Huillier A., Corkum P.B. *Phys. Rev. A*, **49**, 2117 (1994).
22. Carrera J.J., Chu S.-I. *Phys. Rev. A*, **75**, 033807 (2007).
23. Du H., Hu B. *Opt. Express*, **18**, 25958 (2010).
24. Xiang Y., Niu Y., Gong S. *Phys. Rev. A*, **80**, 023423 (2009).
25. Burnett K., Reed V.C., Cooper J., Knight P.L. *Phys. Rev. A*, **45**, 3347 (1992).
26. Feit M.D., Fleck J.A. Jr., Steiger A.J. *J. Comput. Phys.*, **47**, 412 (1982).
27. Keldysh L.V. *Zh. Eksp. Teor. Fiz.*, **47**, 1945 (1964).
28. Antoine P., Piraux B., Maquet A. *Phys. Rev. A*, **51**, R1750 (1995).
29. Frolov M.V., Manakov N.L., Silaev A.A., Vvedenskii N.V. *Phys. Rev. A*, **81**, 063407 (2010).
30. Kim K.T., Kim C.M., Baik M.-G., Umesh G., Nam C.H. *Phys. Rev. A*, **69**, 051805(R) (2004).
31. Lopez-Martens R., Varju K., Johnsson P., Mauritsson J., Mairesse Y., Salières P., Gaarde M.B., Schafer K.J., Persson A., Svanberg S., Wahlström C.-G., L'Huillier A. *Phys. Rev. A*, **94**, 033001 (2005).
32. Sansone G., Benedetti E., Calegari F., Vozzi C., Avaldi L., Flammini R., Poletto L., Villoresi P., Altucci C., Velotta R., Stagira S., De Silvestri S., Nisoli M. *Science*, **314**, 443 (2006).
33. Platonenko V.T. *Kvantovaya Elektron.*, **31**, 55 (2001) [*Quantum Electron.*, **31**, 55 (2001)].
34. Pèrez-Hernández J.A., Roso L., Plaja L. *Opt. Express*, **17**, 9891 (2009).
35. Zhou X.X., Tong X.M., Zhao Z.X., Lin C.D. *Phys. Rev. A*, **71**, 061801(R) (2005).
36. Strelkov V.V. *Phys. Rev. A*, **74**, 013405 (2006).
37. Emelina A.S., Emelin M.Yu., Ryabikin M.Yu. *Kvantovaya Elektron.*, **44**, 470 (2014) [*Quantum Electron.*, **44**, 470 (2014)].
38. Scrinzi A., Geissler M., Brabec T. *Phys. Rev. Lett.*, **83**, 706 (1999).
39. Tong X.M., Lin C.D. *J. Phys. B: At. Mol. Opt. Phys.*, **38**, 2593 (2005).
40. Ammosov M.V., Delone N.B., Krainov V.P. *Zh. Eksp. Teor. Fiz.*, **91**, 2008 (1986).